1993

KEITH D. MILLIS WORLD SYMPOSIUM ON DUCTILE IRON

DUCTILE IRON SOCIETY

Tuesday
through
Friday Noon

OCTOBER 19-22, 1993

CRYSTAL SANDS

HILTON HEAD ISLAND
SOUTH CAROLINA

APPLICATION OF THE SITE THEORY ON THE QUALITY CONTROL OF HEAVY SECTION SPHEROIDAL GRAPHITE CAST IRON

H. Itofuji
Ube Steel Co., Ltd.
Ube City, Japan

INTRODUCTION

This paper is concerned with the application of the SITE THEORY (1, 2, 42, 43) in the quality control of heavy section spheroidal graphite cast iron (spheroidal graphite = s.g.). This of s.g. cast iron requires the highest level of super-integrated quality ever to be covered by any specification. The cast iron involved is a highly stressed major component, the platen of a high pressure plastic injection machine. Fig. 1 shows a single line sketch of this heavy section cast iron. The weight and maximum

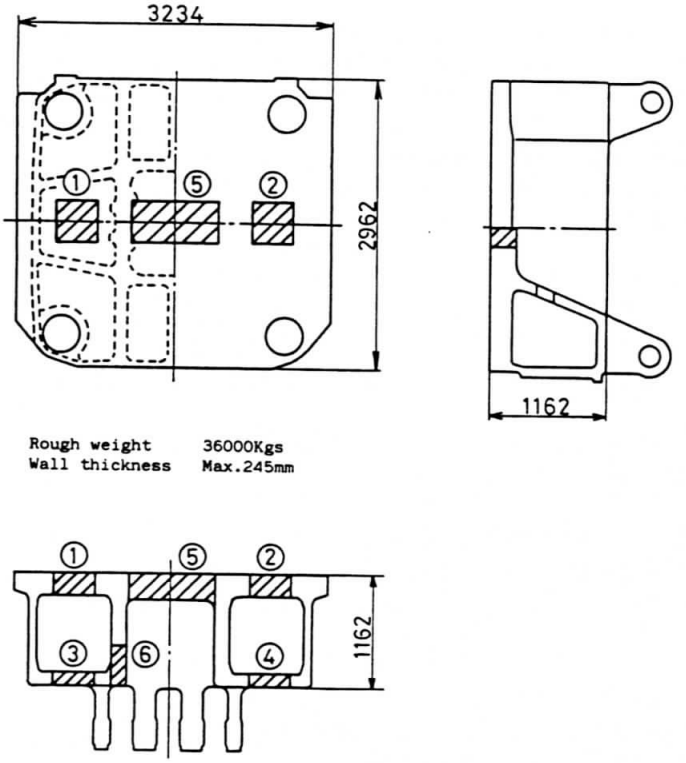

FIG. 1 S.G. Cast Iron by the Application of the SITE THEORY; Part of 2800Tons Die-Clamp-Force Plastic Injection Machine. Cross-Hatched Area Shows Critical Sections of the Cast Iron in Use.

TABLE 1
Mechanical Property Requirements For Heavy Section S.G. Cast Iron Studied in This Paper. (3-5)

Tensile properties[3]				Brinell[3] hardness	Impact[3] value, CVN	Frature toughness	
0.2% Proof stress Kgf/mm²	Tensile strength Kgf/mm²	Elongation %	Reduction in area %	10/3000	Kgf·m/cm²	K1c[4] Kgf/mm$^{3/2}$	J1c[5] Kgf/mm
≒21.2	35.8-36.8	15.0-20.9	15.1-25.3	126-130	2.8-2.9	230-330	3.2-4.4

wall thickness of this cast iron are 36tons and 245mm respectively. At all of the critical sections of the cast iron must conform to required mechanical property specifications, and the matrix must be shrinkage free. Furthermore, the mechanical properties in the cast iron must be equivalent to those required for nuclear waste containers which have the optimum level of quality obtainable in heavy section s.g. cast irons at the present time. The mechanical property requirements are shown in Table 1 (3-5). In this particular case, impact values were not required in application because of the different usage or so it was stated.

In the past, the chemical composition, the spheroidizing treatment and inoculation practice, molding methods, and casting design were not closely controlled. Especially, casting design was adopted from that of cast steel even though the solidification behavior of each metal is quite different. As a result, many unfavorable micro- and macro- defects occurred in heavy section cast irons. A list of these major defects is as follows:

1. Chunky graphite
2. Micro and macro shrinkage
3. Coarse and huge graphite nodules (low nodule count)
4. Graphite flotation and Mg dross
5. Negative chill
6. Swelling and depression

At the present time, using conventional s.g. cast iron production in practice it is no longer possible to meet the most recently up graded specifications for heavy section cast irons as shown in Table 1.

Among the defects noted above, the precipitation of chunky graphite is the most serious and the uncomprehensible problem as it relates to the conventional theories of s.g. formation. When detrimental effect of chunky graphite on the mechanical properties of s.g. cast iron was first recognized, many different methods recommended to overcome this problem (6-27). The majority of these recommendation have only been marginally effective. Many were not, however, always effective in practice.

Shrinkage defects were the next most serious problem. Some investigators (28) only recommended the use of risers to prevent shrinkage in s.g. cast irons. Other investigators (29, 30) recommended both the riserless feeding system design, and the riser feeding system to control shrinkage. Actually, each feeding system design seems to be satisfactory for certain casting design criteria, but not for all.

However, countermeasures to control these two kinds of defects can easily be considered at the same time using the SITE THEORY. Other defects can also be prevented by these countermeasures. Foundry practice used to produce the grade of s.g. cast iron described in Table 1 will be introduced in this paper. The method of production control used is the SITE THEORY. Using this approach, quality can be evaluated on the basis of soundness and mechanical properties. Another s.g. cast iron similar to above will be produced using conventional procedures, and the quality will be compared with the above.

APPLICATION OF THE SITE THEORY IN PRACTICE

The quality control of heavy section s.g. cast irons is based on the solidification control under the SITE THEORY. The controlling factors are listed below;

1. Reduction of the time duration from liquid treatment to the solidification start and finally to its completion.

2. Uniform solidification

3. The effective use of eutectic expansion volume and force.

The First Factor is primarily used to provide an optimum level of s.g. formation, and superior mechanical properties. In order to provide these requirements, the use of chillers and a riserless feeding system is necessary. The correct design and use of chillers in combination with the riserless feeding technique are indispensable to reduce the time interval from beginning of solidification to its completion. Naturally the time interval from the spheroidizing and inoculating treatment to the pouring and secondary oxidation of the liquid metal must be minimized. The most important points are to maintain a sufficient number of magnesium vapor bubbles, and micro segregation of silicon throughout the liquid s.g. iron up until the beginning of solidification. This is to say, that the spheroidization and inoculation effect must be kept at optimum level until solidification begins in order to minimize their fading.

Riserless feeding system design can contribute to the reducing the time interval from pouring to the beginning of solidification and finally to the completion of solidification. (The time interval from liquid to solid state). Under equilibrium conditions, if the chemical composition and temperature of liquid iron can be adjusted to suitable conditions, the volumetric change of s.g. iron on solidification is always positive (29).

This means that riser is not needed theoretically for s.g. cast irons. In this case, carbon equivalent CE (= C% + 4.3%) and eutectic carbide promoting elements such as Cr, Mn, etc. must be held to 4.2-4.3% and to the minimum respectively. The initial temperature of the liquid iron in the mold must be below about 1340°C (2444°F). This procedure makes possible the elimination of the graphite dross defect. The expansion with graphite precipitation always overcomes shrinkage with the reduction of the liquid iron temperature, and austenite precipitation under these conditions. The results of theoretical calculations are shown in Appendix 1, for example. B. Chang originally reported this theory (29) for general small cast irons. In this paper, the theory was modified for heavy section cast irons, and it was presented in a more practical manner.

The Second Factor is primarily utilized to produce shrinkage free s.g. iron. Shrinkage defects reduce mechanical properties of s.g. iron and becomes the initiation point for catastrophic failure of s.g. cast irons in service. For the second factor, the rate of solidification is primarily controlled by the use of chillers, and a riserless feeding system. When solidification is controlled with chillers, it must be uniform throughout the cast iron. The purpose of chillers and riserless feeding system design is to provide uniform solidification. In some s.g. cast irons, uniform solidification is not possible using either chillers or riserless feeding system. In such cases, riser-like pads can be used. However, these pads are not used as risers, but as heat balancers to obtain uniform solidification. Actually, no shrinkage should be observed in either the pads or the s.g. cast iron. Heat insulating materials which can be used in the mold are also available for heat balancing. When heat balancing is used to provide shrinkage free s.g. cast irons, chunky graphite promoting elements such as Ce, Si, Ni, and Ca must be controlled to the minimum. Heat ballancers increase solidification time, and thus promote the formation of chunky graphite.

The Third Factor is a necessary basic condition for over all basic feeding and gating system design. This involves the utilization of eutectic expansion of metal volume (29) and the force (31) generated in undeformable molds. In the case of the third factor, rigid molds such as Furan bonded molds must always be used, and the two mold halves must be clamped together in a very rigid manner. If chillers are used at the parting line of the mold, the formation of a thick solid shell will drive the eutectic expansion force into the mold like the lid on a pressure vessel.

All of the factors must be satisfied in the production of heavy section s.g. cast irons. Otherwise, the high levels of mechanical properties required in these cast irons can not be obtained.

According to the concept of solidification control listed above, the casting design for the actual solidification control of the

cast iron in Fig. 1 is based on the following restrictions and ranges of factors and values:

1. Solidification time - - - - - - - - - - - - - - $10<T<180$min

2. Modified temperature gradient - - - - - - $K = G/R^{1/2}>0.7$

   Area of $K<0.7$ - <2%

   where

   G = temperature gradient (°C/cm)

   R = cooling rate (°C/min)

3. Modulus - $M = V/S>2.5$cm

   where

   V = volume (cm^2)

   S = surface area (cm^2)

4. Safety index for riserless feeding system design (29)

   - - - - - - - - - - - - - - - - $I = M/F>0.5$, $F = (L+W)/T$

   where

   M = modulus (cm) W = width (cm)

   F = shape coefficient T = thickness (cm)

   L = length (cm)

'10. 8. 2
張さんの指摘は、
引用論文が違うと言うこと。
[29]ではない。この当事未発表」

The solidification time values referred to in this paper contains the time duration from pouring to the start of solidification. { This statement can interpreted as meaning that the total solidification time includes both the time interval between the completion of pouring and the liquidus temperature, and the time interval between the liquidus and solidus temperature }. To obtain the aimed for mechanical properties, and the shrinkage free matrix in all critical sections of the cast iron, the feeding system design must satisfy all of the restrictions and the ranges of factors and values required for the critical section of the cast iron. The solidification time affects the morphology of s.g. Other factors affect the occurrence of shrinkage defects. The solidification time and modified temperature gradients were calculated using a computer simulation. A two dimensional finite difference method (2D-FDM) was used as the analysis method. To satisfy each requirement for the factors and values, the effectiveness of chillers and heat ballancing pads were determined by computer simulation. The basic data used in the computer simulation is shown in Table 2.

TABLE 2
Basic Data for Computer Solidification Simulation.

Material	Thermal conductivity Cal/cm^2.sec.°C	Density g/cm^3	Specific heat Cal/g.°C	Latent heat Cal/g	Initial Temp °C	Liquidus Temp °C	Solidus Temp °C	Solid ratio %
Ductile cast iron	0.06	6.90	0.20	50.0	1250	1170	1130	75.0
Chiller	0.08	7.60	0.16	-	20.0	-	-	-
Silica sand	0.003	1.60	2.50	-	20.0	-	-	-
Air	-	-	-	-	20.0	-	-	-

The modulus and safety index for the riserless feeding system design for the cast iron shown in Fig. 2 were calculated by hand.

As a result, the chillers and riserless feeding system design shown in Fig. 2 was found to be suitable for solidification control. Heat ballancing pads were not needed in this case. A large quantity of chillers which have never been considered for s.g. cast iron were needed. The total weight of the chillers was about 40% of the cast iron weight. Solidification at the heaviest section of the cast iron was scheduled as about 150 minutes.

The gating system for this cast iron was designed using Eq. (1);

$$As : Ar : Ac : = 1 : 2 : 0.72 \quad \text{- - - - - - - - - - - - - -} \quad (1)$$

where

As = total cross sectional area of the sprue (cm^2)

Ar = total cross sectional area of the runner (cm^2)

Ac = total cross sectional area of the choke (cm^2)

The total cross sectional area of the choke Ac was determined on the basis of Fig. 3 (32). Others were proportionally based on Eq. (1).

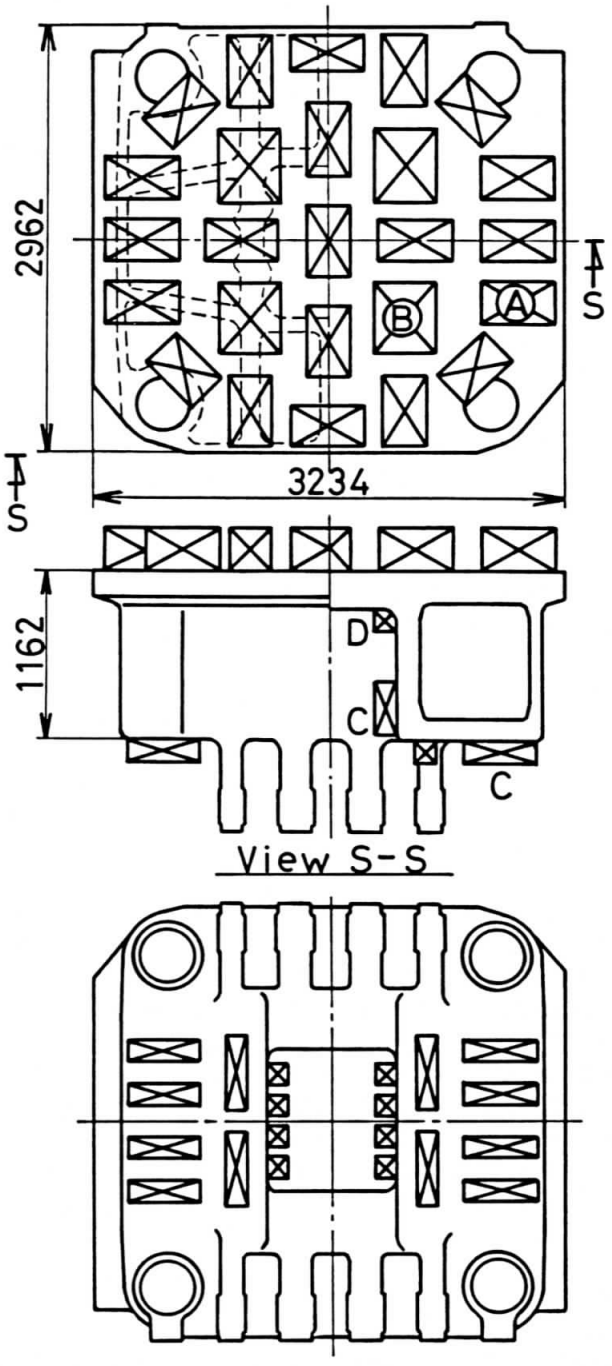

Rough weight	36000Kgs
Gating system	1200Kgs
Flow off	400Kgs
Total weight	37600Kgs
Casting yield	95.7%
Chillers	13000Kgs

FIG. 2 Chillers and Riserless Feeding System Design Obtained by the Application of the SITE THEORY; Chiller A: 300 Square x 500 Thick mm, Chiller B: 400 Square x 500 Thick mm, Chiller C: 150 Square x 500 Length mm and Chiller D: 150mm Cubic and Others.

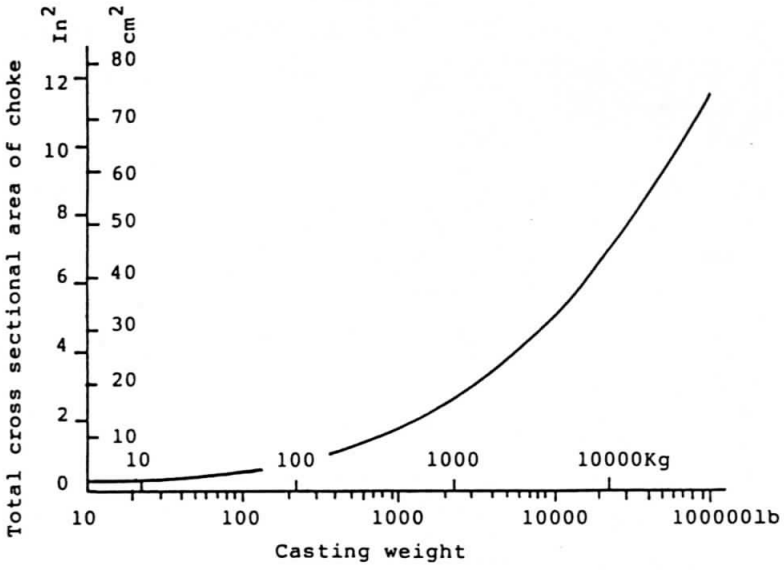

FIG. 3 Guide to Designing the Total Cross Sectional Area of the Choke. (32)

MOLDING AND CLAMPING

Furan bonded silica sand was used for molding. The compressive strength of the Furan bonded silica mold was controlled within the range of 50-60Kgf/cm^2. This is about the same as the maximum eutectic expansion force. The steel flasks used for this mold 4000mm square x 3100mm total hight were made from 30mm thick steel plate. The completed mold was set up in a pouring pit. The side of the flasks were fixed by the walls of the pouring pit. The upper and lower mold halves were clamped together by eight 75mm diameter steel bars. The inside of the mold was dried at 130 °C (266 °F) for 12 hours by the use of electric heat blowers.

MELTING AND LIQUID IRON TREATMENT

A total of forty tons of base iron was melted in an electric arc furnace. The composition of the raw materials used in the furnace charge is shown in Table 3. The base iron charge was melted and brought up to a temperature of 1520 °C (2768 °F). The slag was then removed and the metal was poured into a ladle. At about 1500 °C (2732 °F) the chemical composition of the liquid base iron was adjusted in a simple ladle furnace under argon bubbling. The liquid base iron was then treated with a spheroidizer and inoculant at about 1440 °C (2624 °F) in two ladles by the Sandwich Method after it was transferred to the pouring area. The conditions of each treatment are shown in Table 4.

TABLE 3
Chemical Composition of Melting Materials.

Raw material	Chemical composition (Wt%)							
	C	Si	Mn	P	S	Ca	Al	Bl
Pig iron	4.17	0.26	0.03	0.027	0.015	tr.	tr.	Fe
Steel scrap	0.01	1.11	0.19	0.011	0.008	tr.	tr.	Fe
Fe-Si	0.05	75.7	tr.	0.015	0.005	0.34	1.27	Fe
SiC	60.6	26.4	-	-	0.070	-	0.2	Ash
Carbon	99.0	-	-	-	0.020	-	-	Ash
Graphite	60.0	-	-	-	tr.	-	-	Ash

TABLE 4
Condition of Liquid Treatment and Pouring.

Heat	Alloy (add.Wt%)	Chemical composition (Wt%)							Treatment temp. °C	Reaction time min.	Fading time min.	Pouring temp. °C	Pouring time sec.
		Si	Ba	RE	Ca	Mg	Al	Bl					
Controlled casting	Spheroidizer (1.2)	45.90	-	0.39	2.04	5.86	0.33	Fe	1400	Ladle 1: 2.5	13	1322	76
	Inoculant (0.3)	73.53	1.40	-	2.45	-	1.72	Fe		Ladle 2: 2.5	17	1324	
Conventionally designed casting	Spheroidizer (1.2)	45.04	-	1.90	1.81	5.85	0.38	Fe	1420	Ladle 1: 3.5	18	1350	90
	Inoculant (0.3)	73.53	1.40	-	2.45	-	1.72	Fe		Ladle 2: 3.5	23	1290	

The aimed for chemical composition (Wt%) was as follows:

Carbon	3.40-3.50
Silicon	2.10-2.40
Manganese	<0.35
Phosphorus	<0.050
Sulfer	0.006-0.0013
Calcium	<0.0050
Cerium	<0.010
Magnesium	0.040-0.050
Oxygen	<0.0020
Nitrogen	<0.0090
Other impurities	<0.20
Carbon equivalent	4.2-4.3

The final chemical composition of the s.g. iron was analyzed by an emission spectrochemical analyzer before pouring. The gaseous elements and impurities were analyzed with gas analyzer, and inductively coupled vacuum plasma spectrometer (ICP) respectively after pouring.

POURING

Treated liquid iron was poured into mold via two pouring basins. The pouring conditions are shown in Table 4. The solidification behavior at the heaviest section of the cast iron was measured to determine if it matched the computer simulation. Mold wall movement was also measured optically with a telescope at the top of the upper mold (cope), and visually at the side wall of the lower mold (drag) during pouring and solidification.

KNOCK OUT AND HEAT TREATMENT

After the cast iron was cooled down to about 550°C (1022°F), it was knocked out of the mold and then immediately placed in a furnace and stress-relieved for 8 hours at 560°C (1040°F).

EVALUATION OF THE S.G. CAST IRON

The s.g. cast iron was evaluated on the basis of soundness, and mechanical properties. An evaluation of soundness was made first by nondestructive methods at all critical sections for s.g. quality and for macro defects. The nodularity of s.g. were determined by measuring ultrasonic propagation velocity. Shrinkage defects were evaluated by the ultrasonic testing procedure outlined in (ASTM A609 16/64 in.). According to the requirements in the specification for s.g. cast iron, the evaluation of the mechanical properties shown in Table 5 was conducted in the same critical sections as noted. In addition to the mechanical property requirements shown in Table 1, rotating bending stress and fatigue crack growth rate were also evaluated.

TABLE 5
Test Procedure for Each Mechanical Property.

Test	Specimen	Condition	Tested section
Tensile properties	JIS Z 2201; No.4	Strain speed; 3.3×10^{-3} 1/sec.	(2) (4) (5) (6)
Impact value	JIS Z 2202; No.4	Impact energy; 3Kgf·m Room temp.	(2) (4) (5) (6)
Brinell hardness	Holder of tensile specimen	10mm/3000Kg	(2) (4) (5) (6)
Rotating bending fatigue	JIS Z 2274; No.1-12	Rotating speed; 3000rpm Max.moment; 1.5Kg·m	(1) (3) (5)
Elastic-plastic fracture toughness J1c	ASTM E 813; 1inch B CT (W=2B)	Unloading compliance method	(5)
Fatigue crack growth rate ΔKth	ASTM E 647-78T; 1inch B CT (W=5B)	Direct method	(5)

PRODUCTION AND EVALUATION OF CONVENTIONAL FEEDING SYSTEM S.G. CAST IRON

Another s.g. cast iron of similar weight and thickness was produced using conventional riser design as shown in Fig. 4. Thermal insulators were used as the riser material. The riser design was based on Eq. (2).

$$D = H = 6.2Mc \quad \text{- (2)}$$

where

D = diameter of riser (cm)

H = height of riser (cm)

Mc = modulus of s.g. cast iron (cm)

Other condition were the same as with the controlled feeding system s.g. cast iron. The soundness and mechanical properties for the conventional feeding system s.g. cast iron were evaluated by the same procedure previously used.

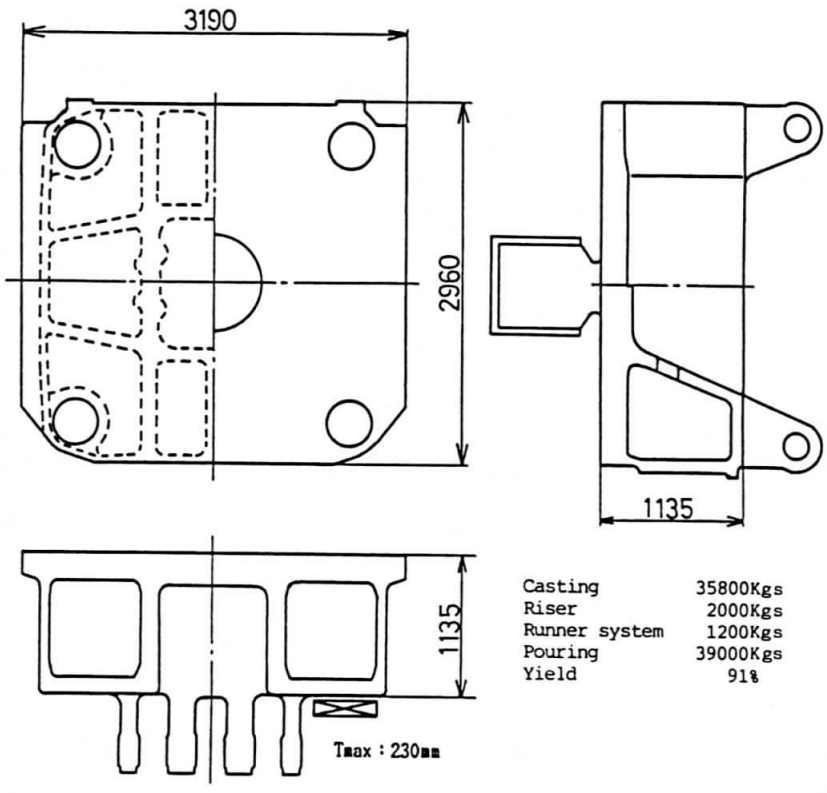

Fig. 4 Feeding System Design Using Conventional Theory; Insulated Riser: 700 Diameter x 700 Height mm, Riser Neck: 420 Diameter x 160 Height mm and Indirect Chiller: 150 Square x 500 Length mm.

EVALUATION OF STANDARD TEST BLOCK

Using the same liquid iron as above two heats were poured into standard test blocks (JIS G 5502 Y-block; B and C types). Tensile and Brinell hardness tests were made on samples from these blocks. Standard testing procedures were used. The test results were compared with those at critical section in each s.g. cast iron.

RESULTS AND DISCUSSIONS

CHEMICAL COMPOSITION

The chemical composition for the controlled and conventionally designed feeding and solidification systems is shown in Table 6. The chemical composition of the first heat was well within those requirements. The chemical composition of the second heat was similar to that of the first heat. However, the silicon and cerium contents were a little higher than those in the first heat.

TABLE 6
Chemical Composition of S.G. Cast Iron at Pouring Basin.

Heat	Chemical composition (Wt%)										(ppm)	
	C	Si	Mn	P	S	Ca	Ce	Mg	CE	OI	O	N
Controlled cast iron	3.46	2.36	0.28	0.045	0.007	0.0024	0.004	0.043	4.25	0.16	2.5	28.0
Conventionally designed cast iron	3.40	2.15	0.35	0.043	0.007	0.0026	0.017	0.044	4.12	0.17	3.5	60.5

CE=TC+1/3Si
OI=Other impurities
=Cr+Ti+Sn+Al+As+Pb+Sb+Bi+Zn+V+Nb

SOLIDIFICATION TIME

The computer simulated and thermocouple measured solidification curves are shown in Fig. 5. The thermocouples used to measure the solidification curves were located below the center of the heaviest section, about three-fourths of the distance toward the center from the chiller face. This location was selected because the computer simulation predicted that hot spots would occur here. The test results showed that there was a good match between the simulation and measurement; the solidification time at the heaviest section was about 150 minutes by the simulation, and about 140 minutes by the measurement. If the solidification time was not controlled, as in the case of the conventionally designed feeding system; complete solidification of the heaviest section would require 12 hours according to the same simulation.

MOLD WALL MOVEMENT

The results of the mold wall movement on both controlled and conventionally feeding systems are shown in Fig. 6. Points 1, 2, 3, and 4 in Fig. 6 were placed where the mold wall movement was measured at the side wall of the drag. The other points were placed where the mold wall movement between the cope and drag was measured on top of the cope.

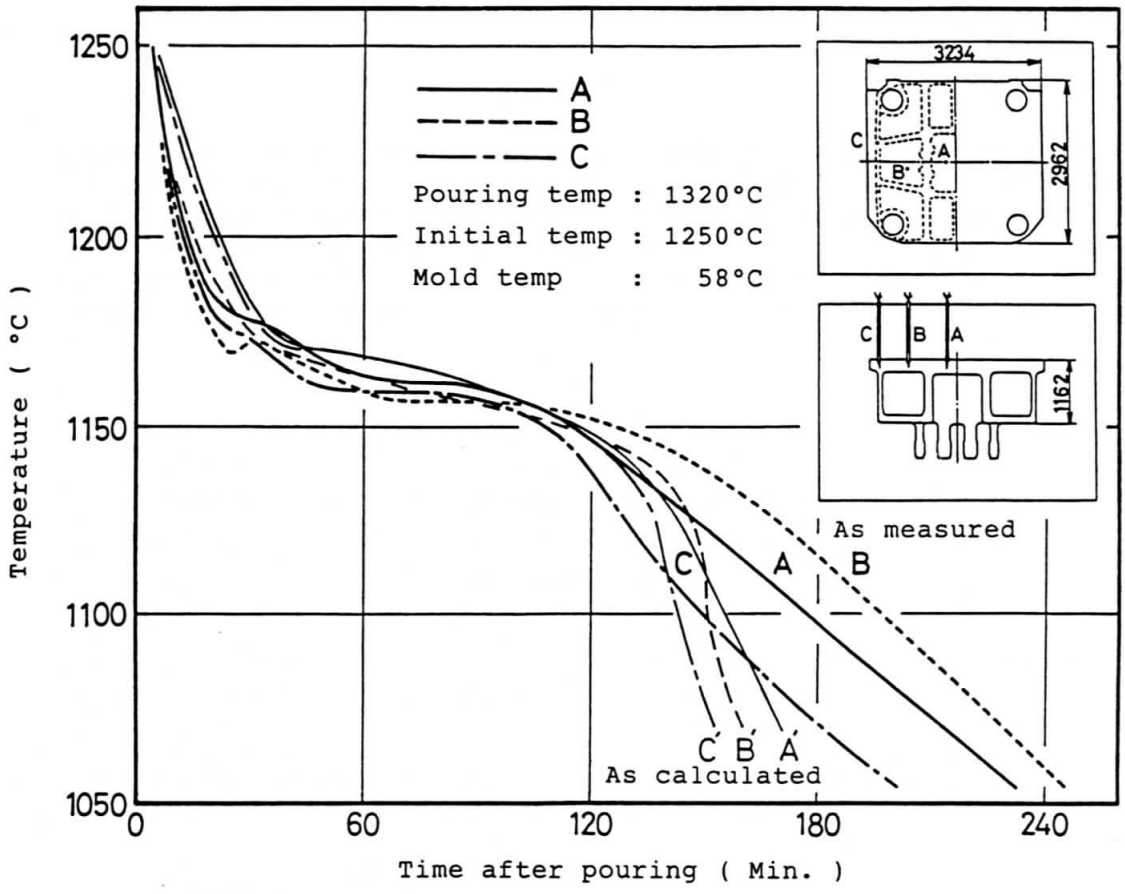

FIG. 5 Cooling Curve for Controlled System S.G. Cast Iron.

The mold wall movement around the side wall of the drag was 0.5-5.5mm during solidification. However, some of the readings might not be representative of the expansion of the s.g. cast iron at each point, because there would be some heat expansion of the sand molds and chillers. Actually, most of the measured points moved continuously, even after the eutectic solidification was completed. The weakest side of the drag wall seemed to receive the eutectic expansion force concentrically. A similar tendency was noted on the side walls of the mold with the conventionally designed feeding system.

A big difference in mold wall movement was observed between the two feeding systems. Toward the cope, there was only a small amount of movement when the controlled feeding system was used (Fig. 6a), but a relatively substantial movement was observed in molds with conventionally designed feeding system (Fig. 6b) just after pouring. This means that buoyancy toward the cope from the liquid iron before solidification and eutectic expansion force toward the same direction as above from the early solidified part in the cast iron can be reduced by the thicker chilled solid shell. This was named as the "lid effect" caused by chillers in this paper.

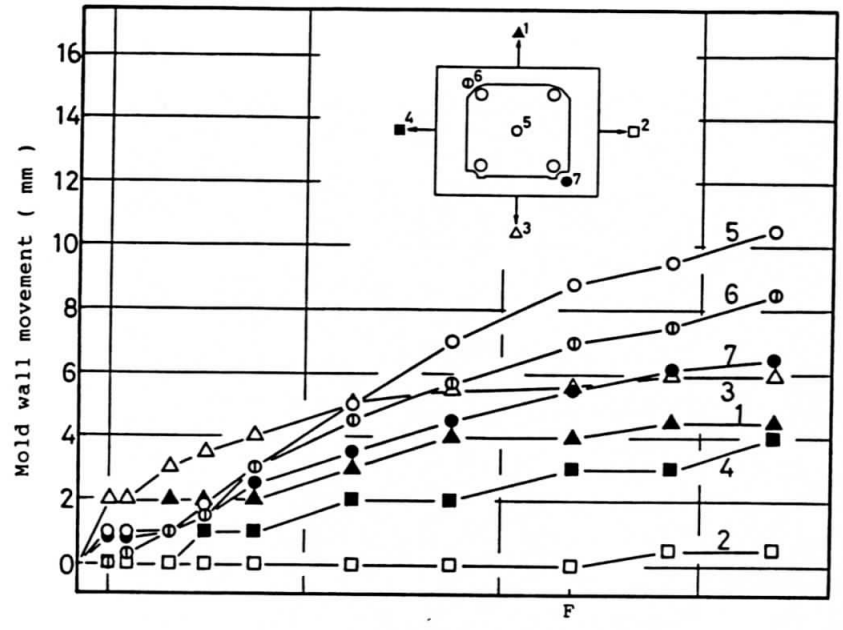

(a)

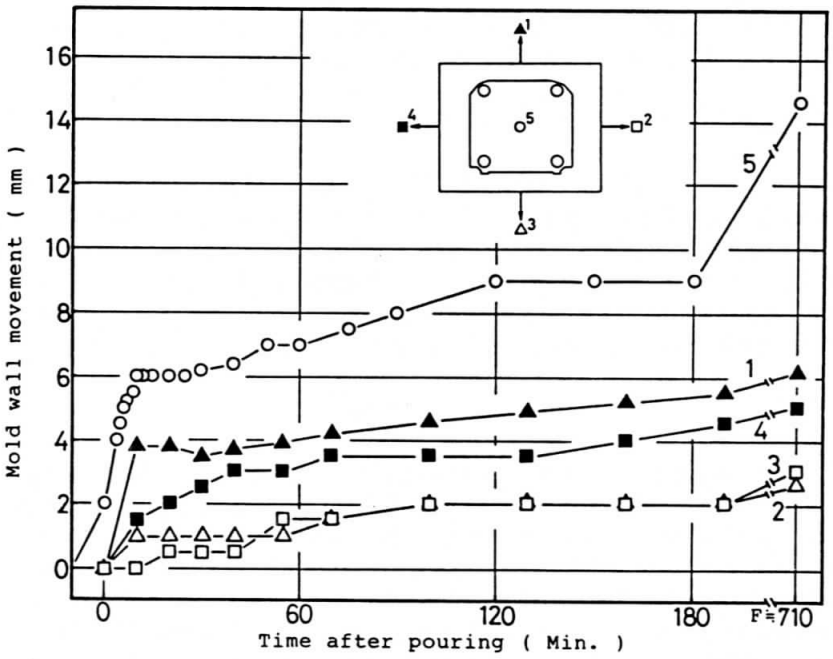

(b)

FIG. 6 Mold Wall Movement; (a) Controlled Feeding System and (b) Conventional Feeding System. Points 1-4 = Side Wall of Drag, Points 5-7 = between Cope and Drag, F = Solidification Time in Heaviest Section.

This "lid effect" has proven to be quite helpful when used with a riserless feeding system as previously noted. Total movement toward the cope during solidification was less in a controlled feeding system than when a conventionally feeding system is used. In each the maximum movement at the completion of solidification was about 9mm and 15mm respectively.

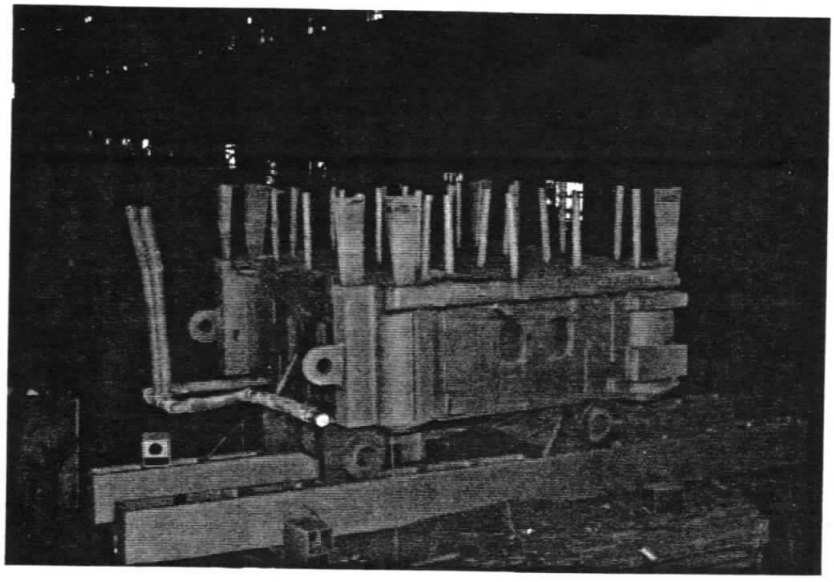

FIG. 7 As-cast Appearance of a Controlled System S.G. Cast Iron After Shot Blasting.

SOUNDNESS AND APPEARANCE

The as-cast appearance of the cast iron produced by the controlled and riserless feeding systems is shown above in Fig. 7. There were no notable surface defects such as shrinkage depressions or swelling at all. Superior appearance was observed. In the case of a conventional feeding system, the maximum swelling of 8mm was observed around the riser neck.

MICROSTRUCTURE

The nodularity of the spheroidal graphite, when it was evaluated by measuring the ultrasonic propagation velocity, showed no difference between critical sections in both cast irons where controlled and conventional feeding systems were used. They were all within the range of 5610-5640m/sec. This is a typical value for heavy section s.g. cast iron in our experience if the nodularity is over 85%. The actual graphite structure was, however, found to be quite different between the two irons. Examination by metallography revealed that the controlled feeding system s.g. cast iron had good nodularity, but that the structure of the cast iron with the conventional risered feeding system contained substantial quantities of chunky graphite. This means that a chunky graphite structure can not be nondestructively

evaluated by ultrasonic propagation velocity. Although a good proportional relationship between ultrasonic propagation velocity and Young's modulus was generally known (35, 36), Young's modulus value was almost equal to each other in the heaviest section of the two cast irons. The typical graphite configuration and microstructure at the heaviest section in each cast iron are shown in Figs. 8 and 9. Results of the micro-examination at section 5 in controlled feeding s.g. cast iron is shown in Table 7.

These two microstructure were hardly distinguishable unless the ultrasonic sensitivity of the bottom echo was not raised to the possible level. The ultrasonic test was conducted on the as-cast surface. A full bottom echo at the heaviest section in controlled feeding system s.g. cast iron could be obtained with 64dB; while that at the heaviest section of the conventionally fed s.g. cast iron could be obtained with 72dB. That is to say, a higher level of sensitivity was needed for chunky graphite structure than s.g. structure. Both bottom echoes shown in the above two sections were determined by the sensitivity pattern as shown in Fig. 10, for example.

TABLE 7
Results of Microstructural Analysis at Section 5 in Controlled Feeding System S.G. Cast Iron.

Layer	Graphite				Ferrite	
	Nodularity %	Nodule diameter μm	Nodule spacing μm	Nodule number N/mm²	Area %	Size μm
Dross (Chiller side)	95	35	105	70	>95	35
Upper	94	50	140	50	>95	50
Middle	95	70	190	30	>90	80
Lower (Sand side)	93	110	250	15	>95	100

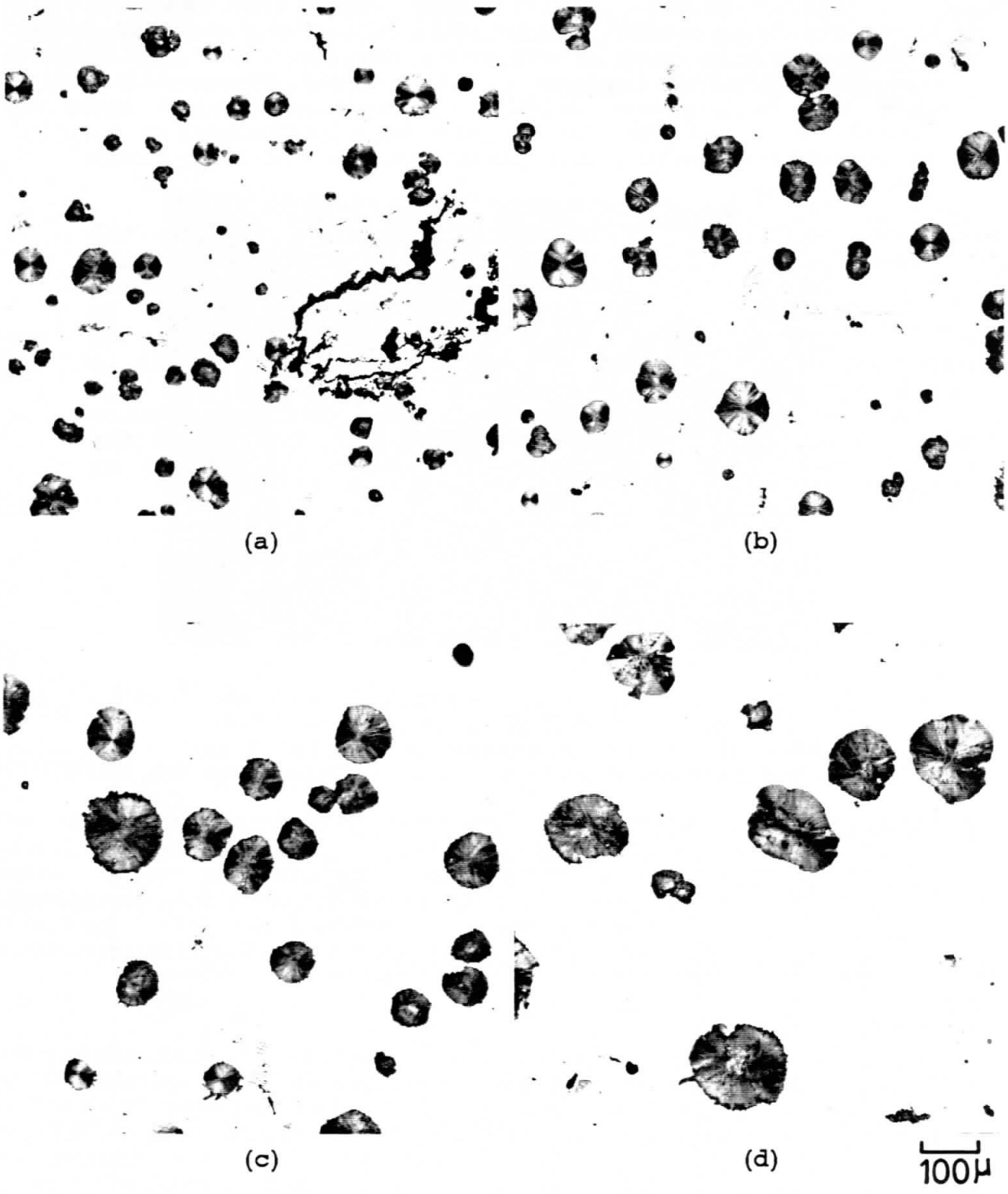

FIG. 8 Microstructure at Section 5 in Controlled Feeding System S.G. Cast Iron (2% Nital Etch); (a) Mg Dross Layer in Machining Allowance on Chiller Side, (b) Upper Layer, (c) Middle Layer, (d) Lower Layer (Sand Side).

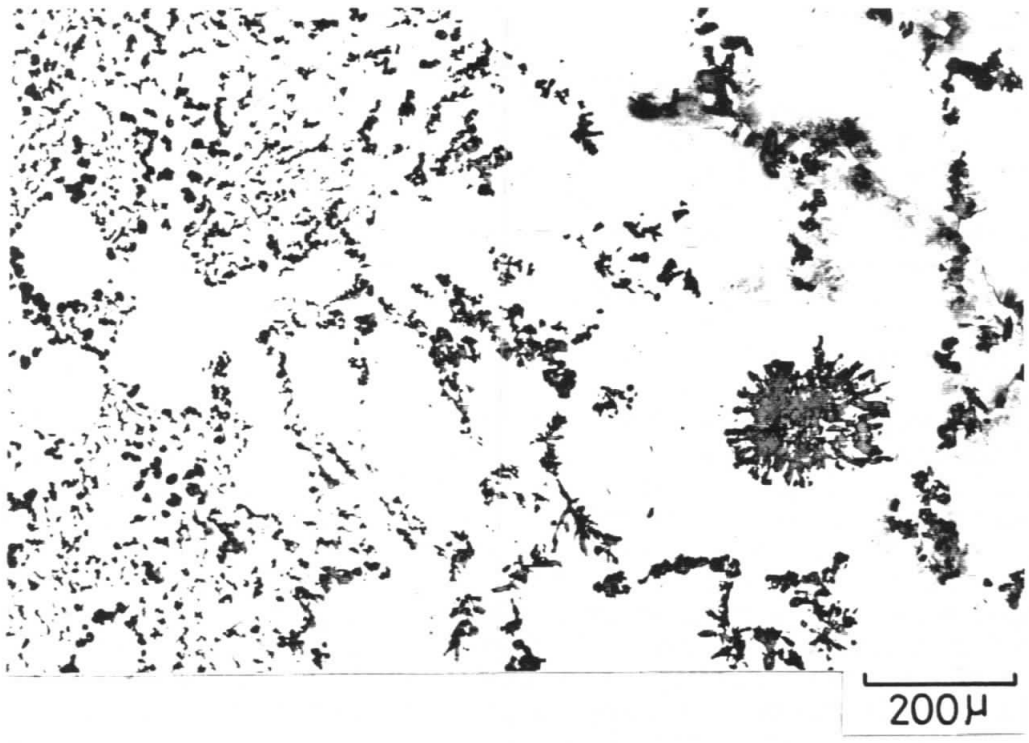

FIG. 9 Microstructure of Chunky Graphite Layer at Thermal Center of Section 5 in Conventional Feeding System S.G. Cast Iron (2% Nital Etch).

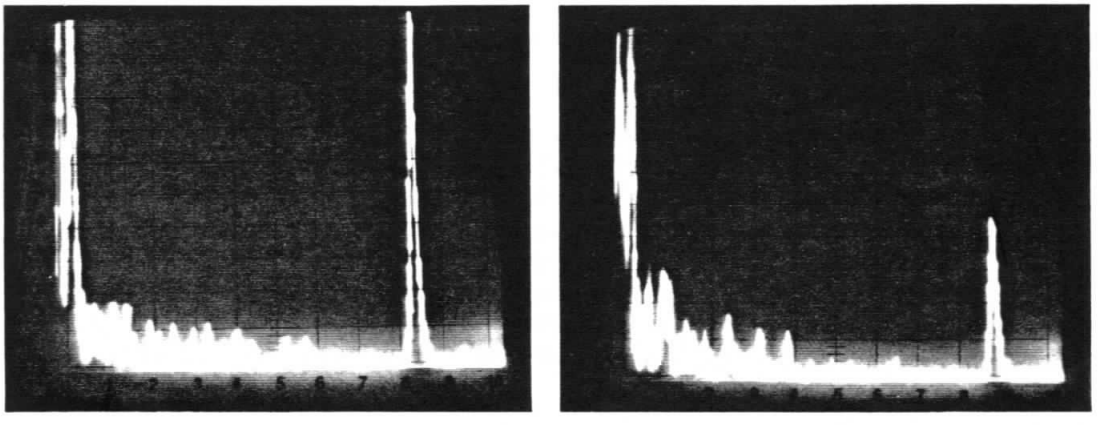

(a) (b)

FIG. 10 Ultrasonic Echo at the Heaviest Section (Sensitivity 64dB); (a) Using a Controlled Feeding System, (b) Using a Conventional Feeding System.

SHRINKAGE AND OTHER DEFECTS INSIDE OF THE CAST IRONS

No defect echo such as that indicating micro and macro shrinkage, macro Mg dross, graphite dross, etc. was observed at all critical sections in the two cast irons by ultrasonic test. Actually, no above mentioned defect was observed in test specimens for each mechanical test when they were sampled at critical sections. However, small quantities of micro Mg dross were observed in the finishing allowance from the heaviest sections of the two s.g. cast irons.

MECHANICAL PROPERTIES

All mechanical properties at the critical sections in controlled and conventional feeding system cast irons are shown in Tables 8 and 9 respectively. Nomenclature for both Tables is described in page 23. All mechanical properties at every section in the case of cast iron where the controlled feeding system was used have superior mechanical properties. There was a tendency for the strength properties to decrease from the chiller side of the mold toward the sand side of the mold in the same section. Cast iron made with the conventionally risered feeding system without direct chillers, however, showed low and inferior values on almost all of the properties evaluated.

TENSILE PROPERTIES

In cast iron made with controlled feeding system, the average values of the tensile properties at every layer in all critical sections were superior to the requirements established in Table 1. The individual values were even at almost every layer. At the magnesium dross layer (Dr) which occurred within the finishing allowance in the heaviest section, tensile strength (TS), elongation (El) and reduction in area (RA) were substantially lower than those at sound layers in the same section, but 0.2% proof stress (PS0.2) showed almost the same level of movement as sound layers.

In cast iron made with conventionally designed feeding system, chunky graphite occurred in most of the layers of critical sections of the cast iron. As a result, tensile properties in these sections were shown to have low values. They were even lower than the values in the above magnesium dross layer. Only in a case where indirect chillers were used in a cast iron made with conventional feeding system it was possible to produce s.g. structure in the cast iron and mechanical properties that meet the requirements in Table 1.

Typical stress strain curves and fracture surfaces of the specimens with representative spheroidal and chunky graphite structures are shown in Figs. 11 and 12 respectively.

TABLE 8
Mechanical Property Test Results in Controlled Feeding System S.G. Cast Iron.

Section		PS0.2	TS	El	RA	HB	CVN	RBS(ER)	J1c(K1c)	E	ΔKth
(2)		25.6	38.9	27.3	23.6	144	1.5				
	U	25.3	38.3	24.6	21.3	146	1.6	18.4(0.47)			
		25.5	39.3	24.6	23.2	147	1.5				
		25.7	39.5	20.3	18.1	143	1.0				
	M	25.9	39.6	21.0	19.1	140	0.9				
		25.6	39.5	21.6	19.4	140	0.8				
		25.9	38.7	21.0	16.9	137	1.0				
	L	26.0	38.0	21.4	18.8	143	1.1				
		26.1	38.8	21.7	20.7	146	1.0				
(4)		26.3	38.9	16.4	15.4	147	1.0				
	U	26.0	39.2	22.4	20.6	138	0.9				
		26.2	38.7	14.8	17.4	137	1.0				
		26.2	39.7	20.6	17.2	140	0.9				
	M	26.1	39.6	18.4	15.9	141	0.9				
		26.0	39.2	16.0	12.1	143	0.8				
		26.1	39.9	25.6	24.1	147	1.4				
	L	26.4	39.9	21.2	22.3	146	1.5	17.0(0.47)			
		26.3	39.9	24.6	23.2	143	1.4				
(5)		24.7	32.8	6.0	8.4	137	1.5				
	Dr	25.3	33.1	6.0	11.1	146	1.4				
		25.3	33.5	4.2	9.8	143	1.5				
		26.0	39.6	24.8	24.1	143	1.3		5.9(333)		
	U	26.3	40.0	25.0	24.1	143	1.3	18.8(0.43)	5.8(330)	17140	28.9
		26.3	39.6	24.0	22.8	140	1.3		6.8(357)		
		26.3	39.6	16.0	13.8	140	0.9		4.6(294)		
	M	26.3	39.6	17.0	16.4	140	0.9		6.3(344)	16940	
		26.6	40.0	19.6	17.7	143	1.0		5.2(313)		
		26.6	39.3	21.4	20.3	140	1.1		5.6(321)		
	L	27.0	39.0	19.0	19.0	143	1.0		6.7(355)	17200	25.4
		27.0	38.7	16.6	16.4	140	1.0		7.0(363)		
(6)	1	25.6	39.1	23.6	18.8	140	1.4				
	U 2	25.8	39.2	23.0	17.9	146	1.1				
	3	26.1	38.9	16.8	14.7	140	1.0				
	1	25.9	39.5	29.2	25.7	142	1.1				
	M 2	25.2	39.4	22.8	19.3	147	1.3				
	3	25.3	39.1	18.0	16.8	143	0.9				
	1	25.7	39.3	25.6	23.5	135	1.1				
	L 2	25.6	39.2	16.2	17.3	140	1.1				
	3	25.9	39.2	19.6	17.6	139	1.1				

TABLE 9
Mechanical Property Test Results in Conventional Feeding System S.G. Cast Iron.

Section		PSO.2	TS	El	RA	HB	CVN	RBS(ER)	J1c(K1c)	E	ΔKth
(2) 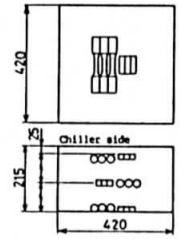	U	27.9	32.2	4.4	2.8	131	0.8				
		27.1	29.6	2.6	1.4	129	0.8	16.0(0.52)			
		27.5	31.2	2.9	1.8	128	-				
	M	27.1	29.6	4.2	4.0		0.7				
		25.5	28.9	3.2	2.6		0.7				
		26.6	29.1	4.0	3.9		0.9				
	L	26.1	39.2	7.8	8.5	137	1.0				
		25.8	36.9	7.8	5.8	126	0.9				
		26.1	37.9	7.8	7.0	137	1.0				
(4) 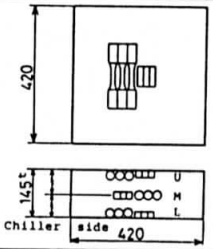	U	25.5	38.8	16.9	15.3		1.0				
		25.1	38.7	14.0	9.6		1.1				
		25.3	38.9	14.1	9.9		0.9				
	M	26.2	36.3	5.6	4.5		0.6				
		26.2	35.3	4.2	3.3		0.6				
		26.2	36.1	5.5	3.3		0.6				
	L	24.5	38.1	23.0	20.6	121	1.3				
		24.4	37.7	21.4	16.6	121	1.6	19.2(0.51)			
		24.5	37.9	21.9	18.3	115	1.3				
(5) 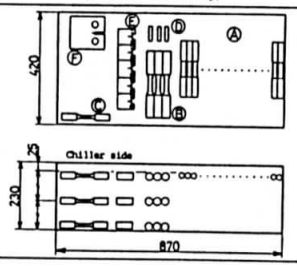	U	26.2	32.0	6.4	4.2	149	1.0				
		26.6	34.7	8.7	4.4	144	1.1	15.7(0.46)			
		26.0	36.1	9.0	6.9	137	1.0				
	M	25.5	28.5	3.6	1.6	149	0.8		3.1(238)	17000	
		25.4	28.0	2.8	1.6	146	1.0		3.5(253)	15990	48.0
		25.0	28.9	3.4	2.1	146	1.1		2.3(205)	17020	
	L	22.6	28.5	5.0	2.1	145	0.7				
		25.8	28.7	5.9	2.0	137	0.9				
		22.7	25.3	4.2	1.7	132	0.9				
(6) 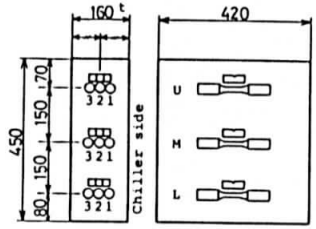	1	26.1	32.8	5.8	5.3		1.0				
	U 2	25.4	30.9	3.4	3.7		1.2				
	3	25.3	32.0	4.3	5.4		1.0				
	1	25.9	32.5	6.0	3.8		0.9				
	M 2	25.0	31.5	3.8	1.7		0.8				
	3	25.9	32.0	4.0	3.2		1.2				
	1	25.6	32.5	5.8	4.4		0.6				
	L 2	24.7	31.0	4.2	1.7		0.8				
	3	25.3	32.5	4.4	3.8		0.7				

*Nomenclature for each mechanical property in Tables 8 and 9

PS0.2: 0.2% proof stress (Kgf/mm^2)

TS : Tensile strength (Kgf/mm^2)

El : Elongation (%)

RA : Reduction in area (%)

HB : Brinell hardness (10/3000)

CVN : Charpy V-notch impact value ($Kgf \cdot m/cm^2$)

RBS : Rotating bending fatigue limit stress (Kgf/mm^2)

ER : Endurance ratio (RBS/TS)

J_{1c} : Elastic plastic fracture toughness (Kgf/mm)

K_{1c} : Stress intensity factor ($Kgf/mm^{3/2}$)

E : Young's modulus (Kgf/mm^2)

ΔKth : Threshold of stress intensity factor ($Kgf/mm^{3/2}$)

U : Upper layer in wall thickness

M : Middle layer in wall thickness

L : Lower layer in wall thickness

Dr : Mg dross layer in wall thickness

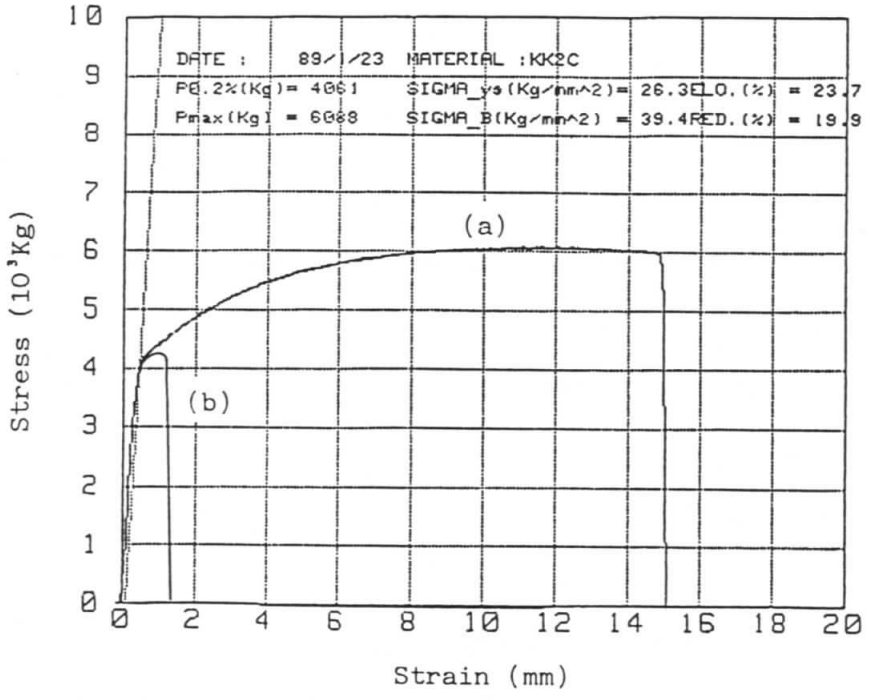

FIG. 11 Comparison of Stress Strain Curves between Two Cast Irons with Different Microstructures; (a) Controlled Feeding System S.G. Cast Iron, (b) S.G. Cast Iron with Chunky Graphite Using a Conventional Feeding System.

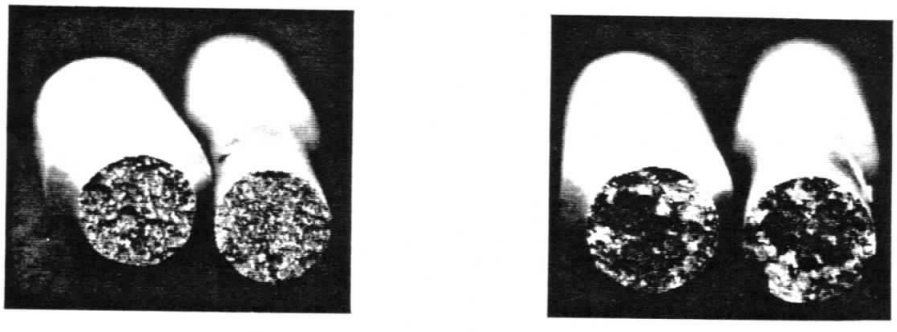

(a) (b)

FIG. 12 Fracture Surfaces of Tensile Test Specimens; (a) Controlled System S.G. Cast Iron, (b) S.G. Cast Iron with Chunky Graphite Using a Conventional Feeding System.

BRINELL HARDNESS

In controlled system s.g. cast iron, the Brinell hardness (HB) was almost uniform among the layers in critical sections. A magnesium dross layer within the finishing allowance did not affect the Brinell hardness. In cast iron made with conventionally designed feeding system, the Brinell hardness was scattered within the range of 115-149. This large scatter is due to the fact that eutectic cells of chunky graphite are large, and the matrix structure is coarse, as shown in Fig. 9.

CHARPY V-NOTCH VALUES

Since high impact strengths were not required for the cast irons made with these feeding systems, no special precautions were taken. When the controlled feeding system was used, Charpy V-notch values (CVN) were lower than the range shown in Table 1. This is because the silicon content was at a higher level than that required for nuclear waste container standards. In nuclear waste container standards, the silicon range is normally 1.8-2.0%. Under such circumstances, the CVN values may be above those shown in this paper. However, in cast iron made with the controlled feeding system, CVN values were still as good as those in the heavy sections. The magnesium dross layer in the finishing allowance did not influence the CVN values because it was located on the chiller side of the cast iron. A good ferrite ratio, graphite nodularity, and nodule size also are responsible good values at the magnesium dross layer.

In cast iron made with conventionally designed feeding system, only the layer of section 4-L showed good CVN values similar to those in cast iron made with controlled feeding system, and all others sections showed poorer values.

ELASTIC PLASTIC FRACTURE TOUGHNESS

To estimate the stress intesity factor (K_{1C}) from elastic plastic fracture toughness (J_{1C}) by Eq. (3), Young's modulus (E) was measured near the J_{1C} specimen for each of the tested layers in section 5.

$$K_{1C} = (E \cdot J_{1C}/1-R^2)^{1/2} \quad - - - - - - - - - - - - - - - \quad (3)$$

where

$$R = \text{Const.} = 0.3$$

In controlled feeding system s.g. cast iron, Young's modulus was almost the same among the layers, and the average was E = 17100Kgf/mm^2. Good R curves were obtained at each layer. The example is shown in Fig. 13. The fracture surface is shown in Fig. 14.

J_{1C} values at every layer were higher than those shown in the in Table 1. This could also be said of the K_{1C} values.

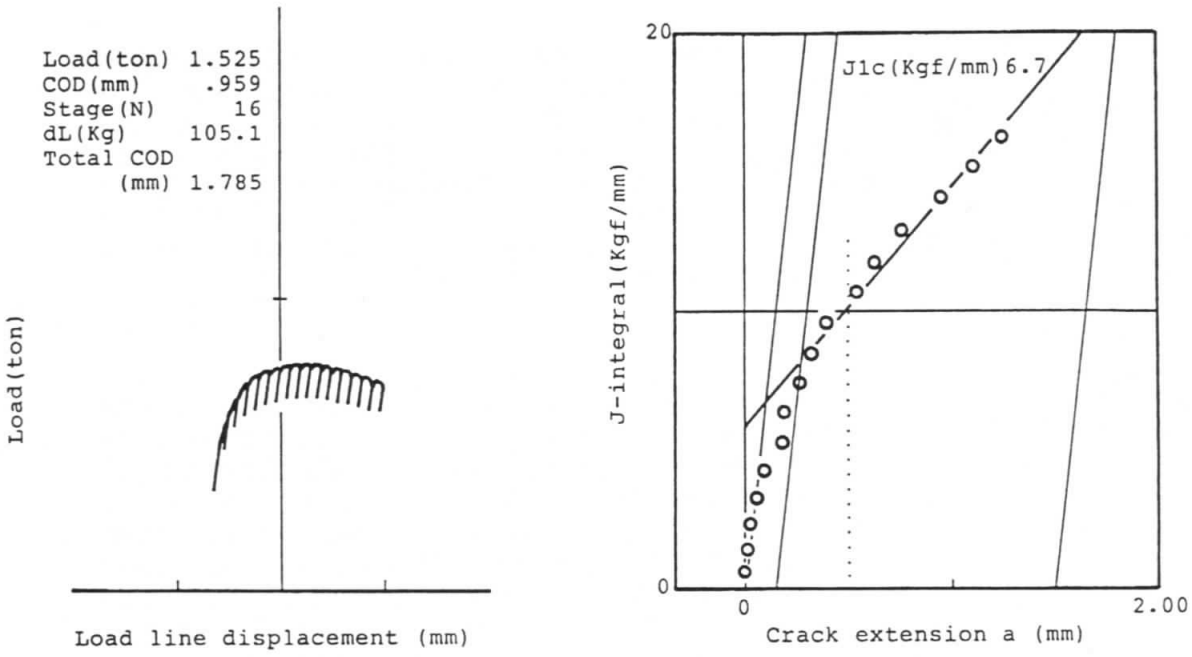

FIG. 13 Example of Data on Elastic Plastic Fracture Toughness Test at Section 5 on the Sand Side in Controlled System S.G. Cast Iron.

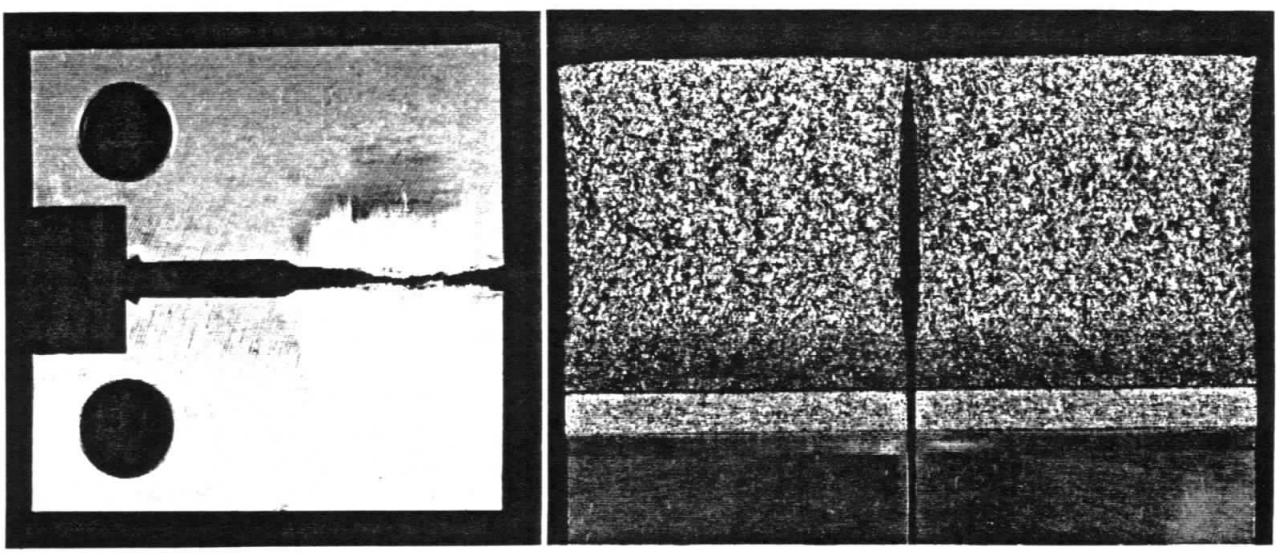

FIG. 14 One Inch CT Specimen for Elastic Plastic Fracture Toughness Test Shown in FIG. 13; (a) Behavior of Fracture Progress, (b) Fracture Surface.

The high level of nodularity made possible by solidification control seems to have a positive influence on the J_{1C} value. K. Kuribayashi et al (37) also mentioned that J_{1C} values linearly increase with the increase in nodularity.

Since nodularity is an important factor in elastic plastic fracture toughness, the values in chunky graphite layer or area were naturally very low.

ROTATING BENDING FATIGUE

The microstructure and soundness at the working surface of the critical section affect the rotating bending fatigue properties in s.g. cast iron used in injection machine components.

The specimens for the rotating bending fatigue test were taken from each surface layer in sections 1, 3, and 5. In sections 1 and 3, the specimens were taken from each surface layer after the finishing allowance was removed. Since the critical sections were completely symmetrical on the shape and dimensions of the s.g. cast irons, the results in sections 1 and 3 are shown in the same columns as sections 2 and 4 respectively in Table 8. The tensile strengths in the surface layers in sections 2 and 4 respectively were used to calculate the endurance ratio (ER = fatigue limit stress/tensile strength) in sections 1 and 3 respectively.

In general, the endurance ratio of heavy section ferritic s.g. cast iron is about 0.42 (38). In the s.g. cast iron produced by controlled feeding and solidification, if this value is applied to the critical sections 2, 4 and 5, the rotating bending fatigue limit stress (RBS) at each section would be 16.3, 16.8 and 16.7Kgf/mm^2 respectively. The actual results showed that both RBS and ER at the surface layers in each examined section were higher than the general values. The excellent microstructure in the cast iron made with controlled feeding and solidification probably is responsible for the improvement in fatigue properties. Other investigators (39, 40) also mentioned this point. A scattering of the fatigue life at each stress limit tends to become larger with the increase in wall thickness. S-N curves in each section are shown in Fig. 15.

When conventional feeding and solidification were used in s.g. cast iron, surface layer 4-L with the s.g. structure was good and had even better fatigue limit stress and endurance ratio than those in cast iron made with controlled feeding and solidification. At the other layers containing chunky graphite structure, however, the presence of chunky graphite did not affect the fatigue limit stress as it decreased the other mechanical properties. The values at each layer in sections 1 and 3 were a somewhat lower than those at the same layer in the controlled feeding system s.g. cast iron.

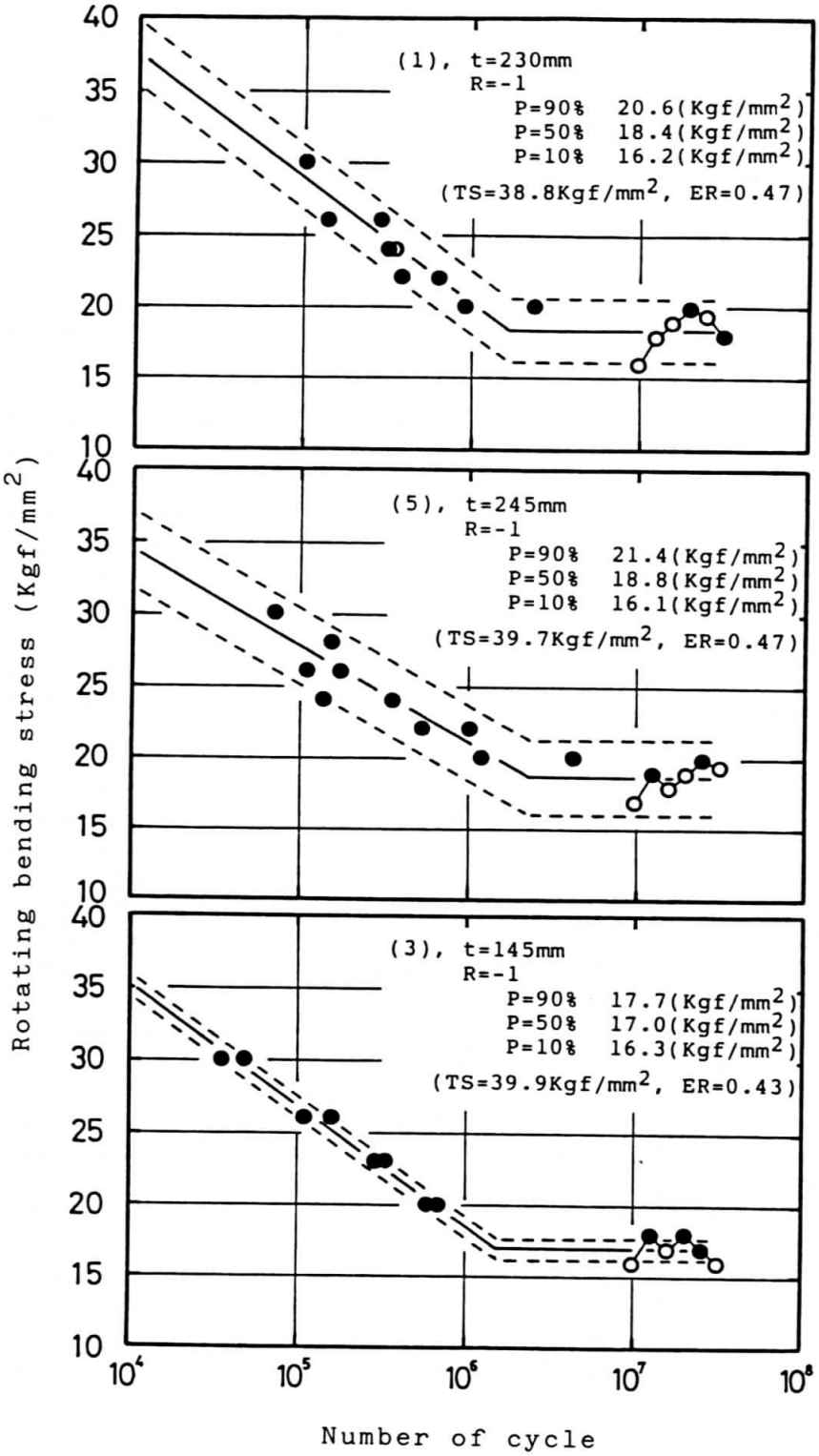

FIG. 15 S-N Curve of Rotating Bending Fatigue Test at Sections 1, 3, and 5 in the cast iron made with Controlled Feeding and Solidification.

FATIGUE CRACK GROWTH RATE

The fatigue crack growth rate test is a new method for the evaluation of the crack sensitivity of s.g. iron, and is not popular among foundry engineers yet. This test is helpful to evaluate the fatigue life of s.g. iron with surface defects such as stress cracks. The general relationship between fatigue crack growth rate (da/dN) and the stress intensity factor range (ΔK) is illustrated in Fig. 16.

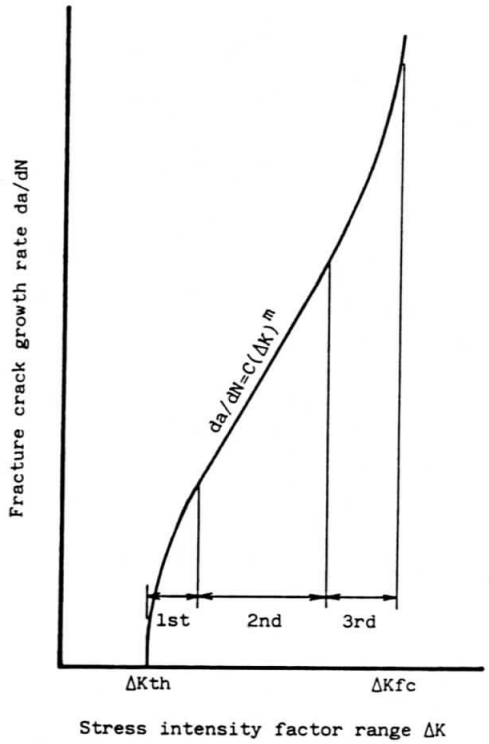

FIG. 16 Illustration of Fatigue Crack Growth Rate da/dN as a Function of Stress Intensity Factor Range ΔK; Threshold ΔKth = Lower Limit, Fatigue Fracture Toughness ΔKfc = Upper Limit.

However, the test condition is not satisfactorily established yet. Actually, da/dN, the threshold (ΔKth) and the fatigue fracture toughness (ΔKfc) were largely changed by certain factors such as test cycle and stress ratio. Especially, the test cycle was sensitive to them. A stable test condition was decided upon after several trials. This test condition is shown in Table 10.

In s.g. cast iron when a controlled feeding system was used, test was conducted in the surface layer on the chiller side and the sand side in section 5.

TABLE 10
Conditions for Fatigue Crack Growth Rate Test.

1:	DATE		;89/10/12
2:	SPECIMEN		; 2-C
3:	COMMENT		; FCD45
4:	Width/Thick	W/B (mm)	; 100.010, 25.400
5:	ELASITISITY	E(kg/mm*2)	; 17100.0
6:	A.Coef	Aa/Ba	; 1.001000, -4.669500
7:		Ca/Da	; 18.4600, -236.8200
8:		Ea/Fa	; 1214.900, -2143.600
9:	K.Coef	Ak/Bk	; .886000, 4.640000
10:		Ck/Dk	; -13.3200, 14.7200
11:		Ek	; -5.6000
12:	FREQ. & PRE CRK	(HZ,mm)	; 5.,100.00
13:	<DL>/Lm	(TON)	; 1.350, .825
14:	FRCT.CK	dL/LLMT	; 0., 5.
15:	CMPL.CAL SPOT NUM:n1~n2		; 5., 20.
16:	END CR(A/W) & DK(MPaRM)		; .75, 89.000
17:	MIN 1SPAN(2&3area)	(mm)	; .30, .30
18:	LAG CRK (INC,DEC)	(mm)	; .20, .20
19:	LOAD AMP	(Ton)	; 5.00
20:	COD AMP	(mm)	; .400

P. Bhandhubanyong (41) reported that Kth value became larger when the solidification rate was slower, and the nodule spacing was greater. In this study, the chiller side, with closer nodule spacing had a slightly higher ΔKth value than that on the opposite side. They were about 28.9 and about 25.4Kgf/mm respectively. The Kth value at the chiller side was almost equal to that thin at section (test block with wall thickness of 20mm) (42). The ΔKfc values at the chiller and sand side were 217.8 and 183.5Kgf/mm respectively. These were both lower than K_{1C} values calculated from J_{1C}. The da/dN value at the

chiller side was smaller than that at the sand side. This means that solidification control is effective for the fatigue crack growth properties. The da/dN-ΔK curves for each layer are shown in Fig. 17. One of the fracture surfaces is shown in Fig. 18.

On the other hand, the same test was conducted at the chunky graphite layer in section 5 in the cast iron made with the conventional feeding system. In spite of the precipitation of chunky graphite, the ΔKth and ΔKfc values were good and about 49.5 and 194.7Kgf/mm$^{3/2}$ respectively. The da/dN value at the chunky graphite layer was much higher than at the above s.g. layers in the cast iron made with a controlled feeding system. The da/dN-ΔK curve and the fracture surface are shown in Figs. 19 and 20 respectively. Chunky graphite with a pearlitic matrix as shown in Fig. 9 may reflect this phenomenon. White network shown in Fig. 20 corresponds to a microstructure containing chunky graphite and pearlitic matrix.

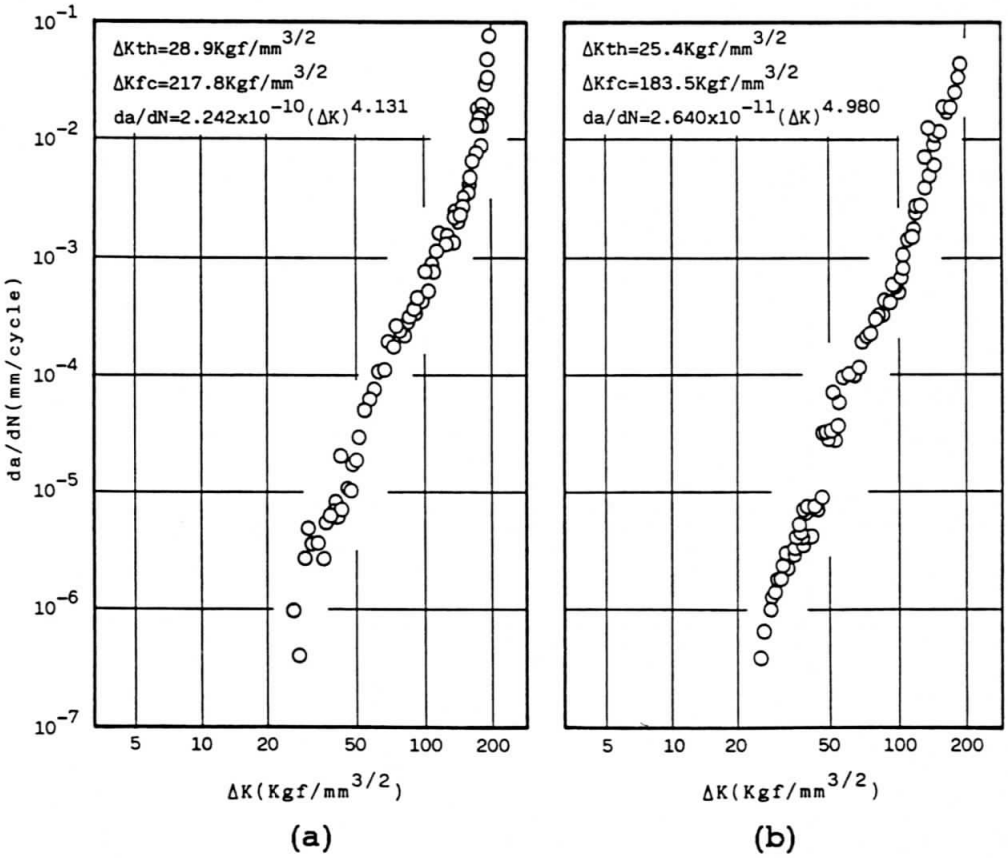

FIG. 17 Fracture Crack Growth Rate da/dN as a Function of Stress Intensity Factor Range ΔK at Section 5 in Controlled System S.G. Cast Iron; (a) Chiller Side, (b) Sand Side.

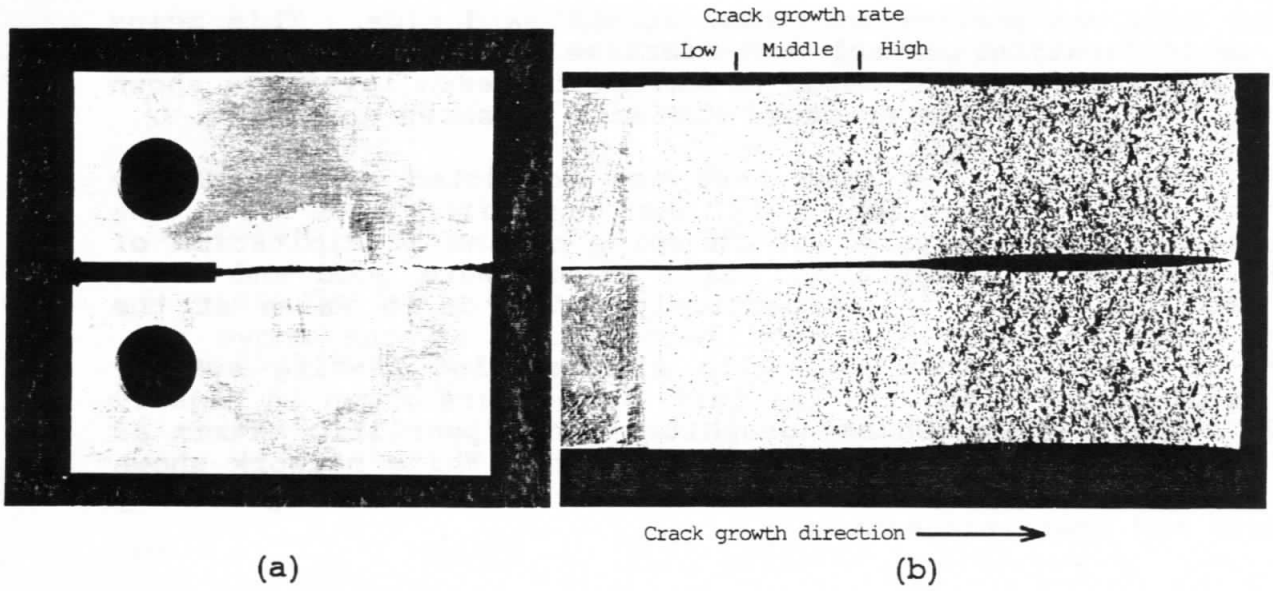

FIG. 18 One Inch 5TCT Specimen for Fatigue Crack Growth Rate Test (Chiller Side Shown in FIG. 17); (a) Crack Growth Behavior, (b) Fracture Surface.

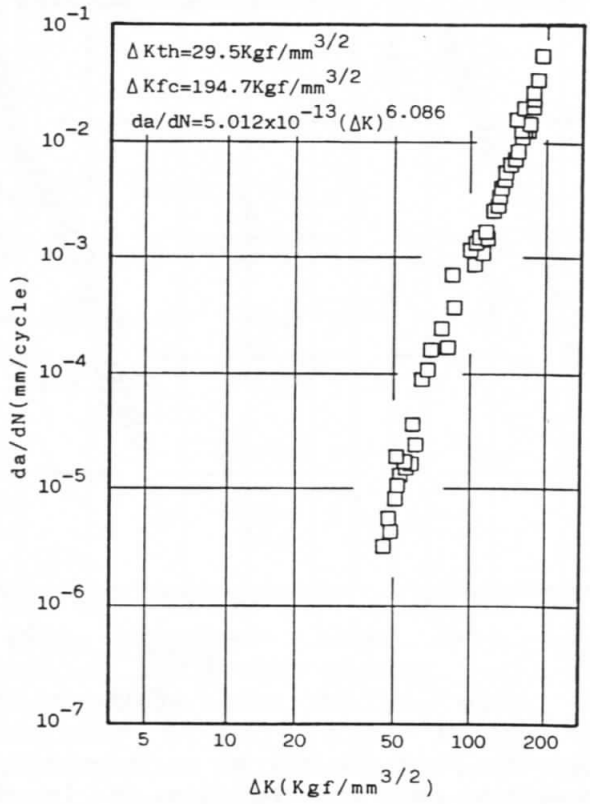

FIG. 19 Fracture Crack Growth Rate da/dN as a ΔK at Section 5 in Chunky Graphite Layer in Cast Iron Using a Conventional Feeding System.

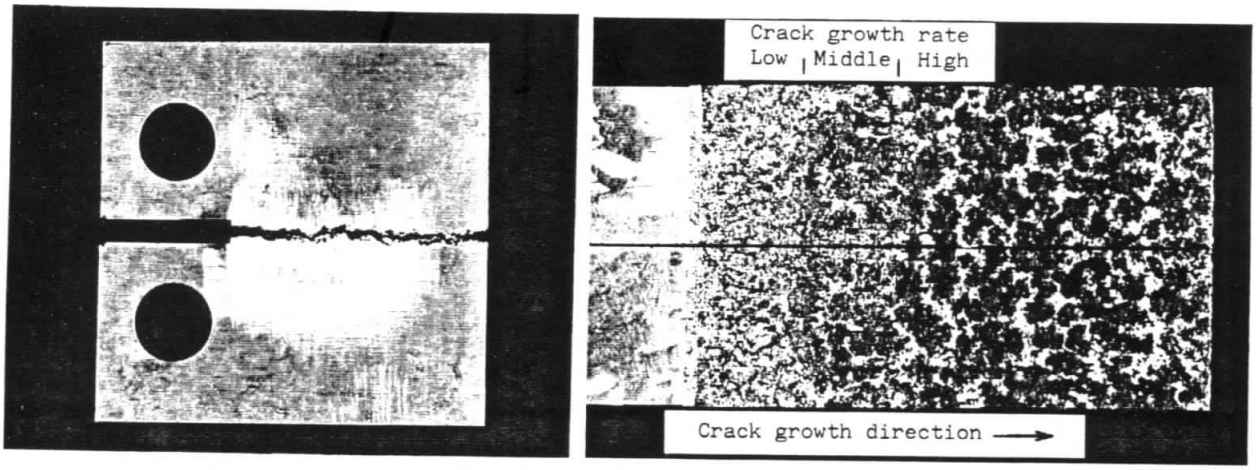

(a) (b)

FIG. 20 One Inch 5TCT Specimen for Fatigue Crack Growth Rate Test (Chunky Graphite Layer); (a) Crack Growth Behavior, (b) Fracture Surface.

MECHANICAL PROPERTIES OF STANDARD TEST BLOCKS

The results of tensile and Brinell hardness tests in standard test blocks are shown in Table 11. The mechanical properties from each test block were about the same as between the two heats. However, there was a big difference between the test

TABLE 11
Results of Mechanical Tests on Standard Test Blocks.

Heat	Test block (JIS G 5502, Y type)	PS0.2	TS	El	RA	HB
Controlled cast iron	1 inch	37.3	65.6	9.4	9.8	247
		38.3	66.9	9.0	7.0	207
	2 inch	35.1	57.2	9.4	8.4	183
		35.1	61.7	9.2	8.4	192
Conventionally designed cast iron	1 inch	34.6	57.2	7.1	8.6	201
		39.2	63.1	6.6	6.0	201
	2 inch	36.5	56.5	11.2	12.4	192
		36.4	59.4	11.2	12.4	207

Nomenclature
PS0.2: 0.2% proof stress (Kgf/mm^2)
TS : Tensile strength (Kgf/mm^2)
El : Elongation (%)
RA: Reduction in area (%)
HB: Brinell hardness (10/3000)

blocks and cast irons in each case. Furthermore, it was impossible to know if chunky graphite will precipitate in s.g. cast irons produced using conventional risered feeding systems on the basis of the mechanical properties from standard test blocks.

As previously mentioned, the nodularity in heavy section cast irons can not be evaluated nondestructively by ultrasonic propagation velocity as in thin sections generally can (33, 34). It is very difficult to distinguish between spheroidal and chunky graphite in heavy sections nondestructively by the sensitivity of ultrasonic echo. In practice, a detailed evaluation of microstructure and mechanical properties in heavy section s.g. cast irons at the present time can only be determined by destructive evaluation of test specimens from cast irons.

CONCLUSIONS

By the application of the SITE THEORY, the quality of heavy section s.g. cast iron could be controlled as designed. Similar s.g. cast iron produced with conventional risered feeding system showed quality levels far below the standard. In practice, the SITE THEORY has been successfully applied to heavy section s.g. cast irons not only for injection machine but also for gas turbine generator, diesel engine generator, marine diesel engine, stone crusher, forging machine, extrusion press, die-casting machine, etc.

REFERENCES

1) H. Itofuji, "Study on Graphite Spheroidization in Cast Irons," Thesis for Doctor's Degree at Department of Metal Science and Technology in Kyoto University, as accepted and printed, Dec. (1993).

2) H. Itofuji, H. Uchikawa, H. Hashimoto and H. Yamada, "Quality Control of Heavy Section Ductile Cast Iron Based on Spheroidization Theory," The 57th World Foundry Congress, Poster Session, Osaka, Japan, Sept. 25-26 (1990), A15.

3) J. M. Motz, "Some Structural and Fracture Mechanical Data of Ferritic Ductile Iron of Great Section Thickness," Seminar: Containers for Radioactive Materials Made from Nodular Cast Iron, Berlin, June 9-10 (1987), P199.

4) R. Helms and J. Ziebs, "Ergebnisse der Werkstoffprofung an Behaltern aus GGG40 in den Jahren bis 1987," Seminar: Containers for Radioactive Materials Made from Nodular Cast Iron, Berlin, June 9-10 (1987), P67.

5) QA Committee (Japan), "Research on Ductile Cast Iron Cask in Japan," Seminar: Containers for Radioactive Materials Made from Nodular Cast Iron, Berlin, June 9-10 (1987), P267.

6) R. K. Buhr, "Vermiculite Graphite Formation in Heavy Section Nodular Iron Castings" AFS Trans., Vol. 76 (1968), P497.

7) R. R. Kust and C. R. Loper, Jr., "The Production of Heavy Section Ductile Iron," AFS Trans., Vol. 76 (1968), P540.

8) T. W. Parks, Jr., N. G. Berry and C. R. Loper, Jr., "The Effect of Solidification Time and Section Size on the Mechanical Properties and Microstructure of High-Carbon Ferrous Alloys," AFS Trans., Vol. 76 (1968), P565.

9) H. Mayer, "Heavy Section Castings in Ductile Iron," AFS International Cast Metals J., Dec. (1976), P21.

10) Y. Maebashi and S. Arimoto, "Influence of Solidification Time on Microstructure and Mechanical Properties of Ferritic Heavy Section Ductile Cast Iron as As-cast Material, Improvement of Ductile Cast Iron," Japan Ductile Cast Iron Association Publish (1982), P303.

11) A. Munnich, "160t Pressenstander," Konstruieren und Giessen Vol. 9, Nr. 1 (1984), P4.

12) M. Sappok, "Different Production Procedures of Casks for Transport and Storage of Spent Nuclear Fuel Elements," Seminar: Containers for Radioactive Materials Made from Nodular Cast Iron, Berlin, June 9-10 (1987), P215.

13) H. Lindscheid and D. Schock, "Verfahren zur Steuerung der

Erstarrungs und Abkuhlungsbedingungen fur Guss-strucke aus Gusseisen," Giesserei, Vol. 75, Nr. 22 (1988), P674.

14) O. Liesenberg and K. P. Wolf, "Effect of Chillers on Ductile and Gray Iron," Foundry Trade J., Vol. 163, Apr. (1988), P292.

15) R. K. Buhr, "The Effects of Pb, Sb, Bi and Ce on Microstructure of Heavy Section Nodular Iron Castings," AFS Trans., Vol. 79 (1971), P247.

16) S. I. Karsay, "Production of Ductile Cast Iron I," (1976), P41.

17) C. W. Thomas, "The Effect of Antimony on the Structure of Low-Magnesium Hypereutectic Irons Containing Proportions of Nodular Graphite," BCIRA J., Vol. 30, Jan. (1982), Repot No. 1453, P36.

18) E. Campomanes, "The Suppression of Graphite Deterioration in Heavy Ductile Iron Castings," Giesserei, Vol. 65, Nr. 20 (1978), P535.

19) S. Morita et al, "Influence of Si on the Formation of Spheroidal Graphite Cast Iron," J. of the ISIJ, Vol. 42, No. 3 (1956), P309.

20) S. I. Karsay and R. D. Schelleng, "Heavy Section Iron Castings Composition Effect on Graphite Structure," AFS Trans., Vol. 69 (1961), P672.

21) R. W. Reesman and C. R. Loper, Jr., "Heavy Section Ductile Iron as Affected by Certain Processing Variables," AFS Trans., Vol. 75 (1967), P1.

22) N. L. Church and R. D. Schelleng, "Detrimental Effect of Calcium on Graphite Structure in Heavy Section Ductile Iron," AFS Trans., Vol. 78 (1970), P5.

23) S. I. Karsay and E. Campomanes, "Control of Graphite Structure in Heavy Ductile Iron Castings," AFS Trans., Vol. 78 (1970), P85.

24) S. Okada and Y. Maebashi, "The Mechanical Properties and Structures of Heavy Ductile Iron Castings," IMONO, Vol. 43, No. 8 (1971), P13.

25) R. Barton, "Nodular Iron: Possible Structural Defects and Their Prevention," Foundry Trade J., Vol. 155, July 14 (1983), No. 3267, P40.

26) T. C. Xi, et al, "The Formation and Prevention of Chunky Graphite in Slowly Solidified Non-Alloy Spheroidal Irons," Fonderie-Fondeur D'aujourd'hui, Vol. 46 (1985), S14.

27) N. Yingyi and Z. Zhu, "A Study of the Rare Earth Effect on Chunky Graphite Formation in Heavy-Section Ductile Iron," the Foundryman, Aug. (1988), P390.

28) N. P. Sinha and V. Kondic, "Theory and Practice of Feeding Spheroidal Graphite Iron Castings," 41st International Foundry Congress, Belgique (1974), Paper No. 7.

29) B. Chang, K. Akechi and K. Hanawa, "Spheroidal Graphite Cast Iron--Basic, Theory and Application," Agne Publish (Japan), (1983), P203.

30) S. I. Karsay, "A Science Based Method of Feeding and Running System Design for Gray-, SG- and CG Iron Castings," FWP Journal, Oct. (1984), P55.

31) K. S. Lee and M. Kayama, IMONO, Oct. 30 (1976), P11./S. I. Karsay, "Ductile Cast Iron 3; Design of Runner System and Riser," QIT Publish (Canada), (1981), P67.

32) S. I. Karsay, "Production of Ductile Cast Iron I," QIT Publish (Canada), (1976), P111.

33) H. Kage and Y. Tanaka, "Evaluation of Cast Iron Quality by Ultrasonic Testing," IMONO, Vol. 56, No. 7 (1984), P24.

34) T. Ohide and K. Ikawa, "Relationship between the Structure of Cast Iron and the Ultrasonic Velocity," IMONO, Vol. 60, No. 2 (1988), P116.

35) A. Orlikowski, W. Pittack and G. Buchholy, "Ultrasonic Immersion Auto Test Instrument for Inspection on Spheroidal Graphite Cast Iron, Part 3; Evaluation of Test Results," Giesserei, Vol. 76, Nr. 20 (1989), P701.

36) T. Abe, S. Zhung-Wang and K. Ikawa, "Effects of Structure and Mechanical Properties on the Sound Velocity in Cast Iron," IMONO, Vol. 57, No. 6 (1985), P13.

37) K. Kuribayashi et al, "Elastic-Plastic Fracture Toughness in Nodular Cast Iron," ISIJ, Vol. 69, No. 6 (1983), P157.

38) K. B. Palmer, "Effect of Cast Section Size on Fatigue Properties and the Prevention of Corrosion Fatigue of Nodular Irons," the British Foundryman, Vol. 75, Nov. (1982), P201.

39) T. Shiota and S. Komatsu, "Influence of Graphite Nodule Diameter on Fatigue Strength and Crack Propagation Behavior of Ferritic Spheroidal Graphite Cast Irons under Rotational Bending," IMONO, Vol. 54, No. 7 (1982), P14.

40) A. G. Fuller, "Effect of Graphite Form on Fatigue Properties of Pearlitic Ductile Irons," AFS Trans., Vol. 85 (1977), P527.

41) P. Bhandhubanyong, Paper for PhD degree, Tokyo University (1983).

42) "Research on Substantial Strength of Cast Iron--On Fatigue Crack Growth Rate Test of Cast Iron Products," the Material Process Technology Center, (1985), Report No. 313, Series 4.

43) H. Itofuji and H. Uchikawa, "Formation Mechanism of Chunky Graphite in Heavy-Section Ductile Cast Irons," AFS Trans., Vol. 98 (1990), P429.

44) H. Itofuji, "Magnesium Map of the Spheroidal-graphite Structure in Ductile Cast Irons," CAST METALS, Vol. 5, No. 1 (1992), P6 / Discussion , Vol. 5, No. 4 (1993), P235.

29) Bakk Chang, " Ductile iron Castings with No-Riser", JACT NEWS, No.419(1985)P1.

App. 1
Theoretical Volumetric Change of S.G. Iron from Pouring to the End of Solidification.

	CE=C+1/3Si	4.2	4.2	4.3	4.3
	(C, Si)	(3.6, 1.8)	(3.5, 2.1)	(3.6, 2.1)	(3.5, 2.4)
	C_γ	1.72	1.67	1.67	1.62
	Ce	3.67	3.57	3.57	3.47
Ti=1400 ℃	1.S_ℓ	-3.75	-3.75	-3.75	-3.75
	2.Epg(Ep_γ)	(-0.13)	(-0.13)	+0.11	+0.11
	3.S_γ	-3.31	-3.31	-3.30	-3.30
	4.Eeg	+6.48	+6.32	+6.32	+6.15
	1+2+3+4	-0.71	-0.87	-0.62	-0.79
	1+3+4	-	-	-0.73	-0.90
Ti=1350 ℃	1.S_ℓ	-3.00	-3.00	-3.00	-3.00
	2.Epg(Ep_γ)	(-0.13)	(-0.13)	+0.11	+0.11
	3.S_γ	-3.33	-3.33	-3.33	-3.33
	4.Eeg	+6.53	+6.37	+6.37	+6.20
	1+2+3+4	+0.07	-0.09	+0.15	-0.02
	1+3+4	-	-	+0.04	-0.13
Ti=1300 ℃	1.S_ℓ	-2.25	-2.25	-2.25	-2.25
	2.Epg(Ee_γ)	(-0.13)	(-0.13)	+0.11	+0.11
	3.S_γ	-3.36	-3.36	-3.35	-3.36
	4.Eeg	+6.59	+6.42	+6.42	+6.25
	1+2+3+4	+0.85	+0.68	+0.93	+0.75
	1+3+4	-	-	+0.82	+0.64
Ti=1250 ℃	1.S_ℓ	-1.50	-1.50	-1.50	-1.50
	2.Epg(Ep_γ)	(-0.13)	(-0.13)	+0.11	+0.11
	3.S_γ	-3.38	-3.38	-3.38	-3.38
	4.Eeg	+6.64	+6.47	+6.47	+6.29
	1+2+3+4	+1.63	+1.46	+1.70	+1.52
	1+3+4	-	-	+1.59	+1.41
Ti=1200 ℃	1.S_ℓ	-0.75	-0.75	-0.75	-0.75
	2.Epg(Ep_γ)	(-0.13)	(-0.13)	+0.11	+0.11
	3.S_γ	-3.41	-3.41	-3.40	-3.40
	4.Eeg	+6.67	+6.52	+6.52	+6.34
	1+2+3+4	+2.38	+2.23	+2.48	+2.30
	1+3+4	-	-	+2.37	+2.19

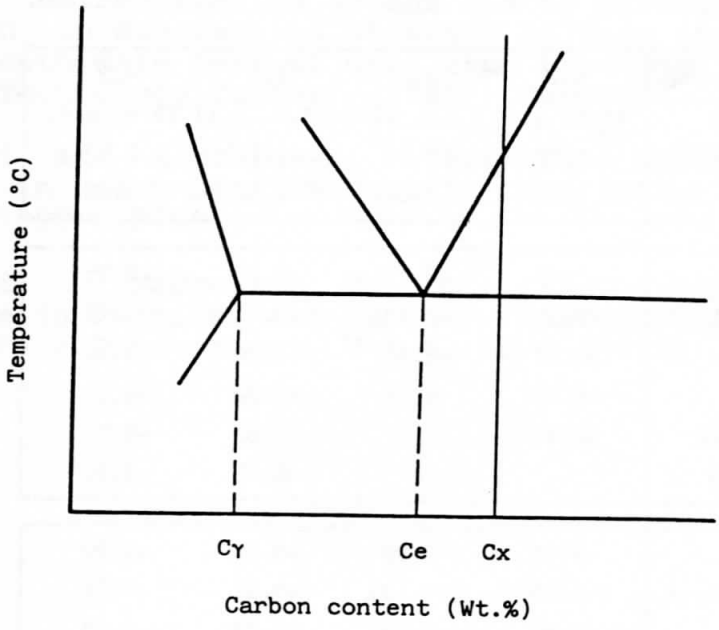

App. 1-1 Illustration of Fe-C equilibrium phase diagram.

*Nomenclatures for Apps.1 and 1-1

CE = Carbon equivalent (Wt.%) = C + 1/3Si

C_γ = Carbon solution in austenite (Wt.%) = 2.045 - 0.178Si

Ce = Carbon content at eutectic point (Wt.%) = 4.27 - 1/3Si

Cx = Carbon content (Wt.%)

S_ℓ = Liquid shrinkage (Vol.%) = 1.5(Ti - 1150)/100

where;

Ti = Initial liquid temperature in mold (°C)

1.5/100 = Liquid shrinkage ratio (%/°C)

1150 = Finish temperature of solidification (°C)

Epg = Expansion by precipitation of primary graphite (Vol.%)

$= 3.4[(Cx - Ce)/(100 - Ce)] \cdot 100$

where;

3.4 = Specific gravity of austenite/Specific gravity of graphite

= 7.66/2.25

Ep_γ = Shrinkage by precipitation of primary austenite (Vol.%)

$= 3.5[(Ce - Cx)/(Ce - C_\gamma)]$

where;

3.5 = Solidification shrinkage of liquid iron (Vol.%)

= Shrinkage by precipitation of primary austenite (Vol.%)

S_γ = Shrinkage by precipitation of eutectic austenite (Vol.%)

$= 3.5(1 - S_\ell/100)[(100 - Cx)/(100 - Ce)][(100 - Ce)/(100 - C_\gamma)]$

Eeg = Expansion by precipitation of eutectic graphite (Vol.%)

$= 3.4(1 - S_\ell/100)[(100 - Cx)/(100 - Ce)][(Ce - C_\gamma)/(100 - C_\gamma)] \cdot 100$